AGU PUBLICATIONS

JGR

Journal of Geophysical Research: Atmospheres

RESEARCH ARTICLE
10.1002/2016JD026093

Key Points:
- By weakening entrainment over land, the dry bias over land is reduced
- Anomalous precipitation maximum over the west Atlantic results from a too weak sensitivity to the monsoon circulation
- Biases over land and over ocean have minimal impact on each other

Correspondence to:
A. C. Siongco,
siongco1@llnl.gov

Citation:
Siongco, A. C., C. Hohenegger, and B. Stevens (2017), Sensitivity of the summertime tropical Atlantic precipitation distribution to convective parameterization and model resolution in ECHAM6, *J. Geophys. Res. Atmos.*, *122*, 2579–2594, doi:10.1002/2016JD026093.

Received 14 OCT 2016
Accepted 7 FEB 2017
Accepted article online 9 FEB 2017
Published online 3 MAR 2017

Sensitivity of the summertime tropical Atlantic precipitation distribution to convective parameterization and model resolution in ECHAM6

Angela Cheska Siongco[1,2], Cathy Hohenegger[1], and Bjorn Stevens[1]

[1] Max Planck Institute for Meteorology, Hamburg, Germany, [2] Now at Lawrence Livermore National Laboratory, Livermore, California, USA

Abstract A realistic simulation of the tropical Atlantic precipitation distribution remains a challenge for atmospheric general circulation models, owing to their too coarse resolution that makes it necessary to parameterize convection. During boreal summer, models tend to underestimate the northward shift of the tropical Atlantic rain belt, leading to deficient precipitation over land and an anomalous precipitation maximum over the west Atlantic ocean. In this study, the model ECHAM6 is used to test the sensitivity of the precipitation biases to convective parameterization and horizontal resolution. Two sets of sensitivity experiments are performed. In the first set of experiments, modifications are applied to the convection scheme in order to investigate the relative roles of the trigger, entrainment, and closure formulations. In the second set, the model is run at high resolution with low-resolution boundary conditions in order to identify the relative contributions of a high-resolution atmosphere, orography, and surface. Results show that the dry bias over land in the model can be reduced by weakening the entrainment rate over land. Over ocean, it is found that the anomalous precipitation maximum occurs because of model choices that decrease the sensitivity of convection to the monsoon circulation in the east Atlantic. A reduction of the west Atlantic precipitation bias can be achieved by (i) using a moisture convergence closure, (ii) increasing the resolution of orography, or (iii) enhancing the production of deep convection in the east Atlantic. The biases over land and over ocean do not impact each other.

1. Introduction

The ability of models to simulate the summertime precipitation distribution in the tropical Atlantic rests on at least three factors: the simulated surface winds and temperatures, the convective parameterization, and the model resolution. Coupled general circulation models (CGCMs) generally fail in the first aspect, as most of them lack even basic features of the summertime tropical Atlantic climate, such as the rapid cooling of sea surface temperatures (SSTs) at the eastern equatorial Atlantic and the concurrent northward shift of the rain belt [*Davey et al.*, 2002; *Cook and Vizy*, 2006; *Richter and Xie*, 2008; *Roehrig et al.*, 2013]. When prescribed with observed SSTs, atmospheric GCMs (AGCMs) exhibit marked improvements, especially in the West African monsoon circulation [*Hourdin et al.*, 2009; *Xue et al.*, 2010]. However, despite the improved circulation, AGCMs continue to suffer from biases in precipitation over the tropical Atlantic sector. Over ocean, models tend to misplace the summertime Atlantic Intertropical Convergence Zone (ITCZ) maximum over the west Atlantic, in contrast to the eastward maximum in the observations [*Biasutti et al.*, 2006; *Siongco et al.*, 2015]. Over land, models have a tendency to underestimate precipitation over regions such as the Sahel and the Amazon [*Hourdin et al.*, 2009; *Richter and Xie*, 2008]. Diagnosing the root cause behind these biases requires us to look into the roles of the second and third aspects—the convective parameterization and model resolution.

The convective parameterization determines the occurrence of convection within a model grid box. It has three main components: (1) the trigger, which decides whether convection is possible, (2) the cloud model, which predicts the resulting vertical profiles of heating and moistening due to convection, and (3) the closure, which sets the strength of convection. The choice of the convection scheme, as well as the formulation of its different components, can strongly impact the resulting precipitation distribution. Many studies have, for instance, revealed that by switching to a different convective paramaterization, or by simply changing one component such as the entrainment rate, a shift from a single to a double ITCZ occurs in an aqua-planet model [*Chao and Chen*, 2004; *Liu et al.*, 2010; *Moebis and Stevens*, 2012; *Oueslati and Bellon*, 2013].

Independently of the convection scheme, *Siongco et al.* [2015] found that horizontal resolution has an influence on the position of the summertime Atlantic ITCZ. Models with high resolution correctly place the ITCZ maximum over the east Atlantic, whereas models with low resolution tend to have unrealistically high rainfall rates over the west Atlantic. Specific reasons behind the resolution dependence of the Atlantic ITCZ have not been explained yet, and various possible drivers exist. *Schiemann et al.* [2013] showed that the resolution of coastlines has a pronounced effect on the land-sea partitioning of surface latent heat flux in their general circulation model, especially over the Maritime continent. The resolution of orography might also play a role, through its impact on the strength of orography-induced forcings on the circulation. For instance, over East Africa, a better resolved orography results in a stronger Somali jet [*Johnson et al.*, 2016]. Another possible driver is the resolution of the atmospheric grid, which can change the behavior of the parameterization schemes, depending on the model configuration [*Duffy et al.*, 2003; *Landu et al.*, 2014].

In this study, we investigate how assumptions implicitly made in the employed convective parameterization and horizontal resolution impact the resulting summertime precipitation distribution over the tropical Atlantic sector. We are interested in two particularly prominent biases during boreal summer—the anomalous westward Atlantic ITCZ maximum over ocean and the dry bias over land. We aim to answer the following questions: (1) To what extent can the biases be attributed to the different components of the convection scheme (the trigger, entrainment, and closure) and different aspects of the resolution (land surface, orography, atmospheric dynamics)? and (2) Are biases over ocean coupled with biases over land? By better understanding these aspects, we aim at better understanding how the convection scheme interacts with the atmospheric flow and hence what mechanisms control the precipitation distribution over the Atlantic.

Using the model ECHAM6, two sets of sensitivity experiments are performed. In the first set of experiments, different parts of the convection scheme—the trigger, entrainment, and closure—are modified during summer in order to test how the precipitation responds to changes in each component. The modifications are applied separately over land and over ocean, allowing us to study the interaction between continental and oceanic precipitation biases. In the second set of experiments, the model is run at high resolution and combined with low-resolution boundary conditions in order to identify the relative contributions of a high-resolution atmosphere, orography, and land surface.

The outline of the paper is as follows: section 2 describes the model and the first set of sensitivity experiments with the convection scheme. In section 3, we discuss impact of the convection scheme and its different components on the precipitation biases over land, over ocean, and the interaction between land and ocean biases. The resolution dependence of the biases is presented in section 4, which starts with a description of the second set of experiments, followed by a discussion on the relative roles of a high-resolution atmosphere, orography, and surface. Conclusions are given in section 5.

2. Methods

2.1. Model

Numerical simulations are performed using the atmospheric general circulation model ECHAM version 6.2. This model version is similar to the one described in *Stevens et al.* [2013], except that errors in the implementation of the cloud cover scheme have been fixed. ECHAM6 uses a dry spectral transform dynamical core and a transport model for different water species and chemical tracers. The model supports triangular truncations at T31, T63, T127, and T255, corresponding to grid point resolutions of 3.75°, 1.875°, 0.93°, and 0.47°, respectively. It employs a hybrid sigma-pressure coordinate system, with either 47 or 95 levels in the vertical. The two vertical grids share the lowermost 12 levels up to 611 hPa, as well as the uppermost layer centered at 1 hPa. The model includes a suite of physical parameterizations for the representation of diabatic processes [*Stevens et al.*, 2013]. As described in more detail in *Moebis and Stevens* [2012], the default convective parameterization in ECHAM6 is based on a bulk mass flux scheme developed by *Tiedtke* [1989], with modifications for deep convection by *Nordeng* [1994]. Hereafter, we will refer to the default scheme as the Nordeng scheme. The Nordeng scheme considers a single entraining-detraining plume. Mixing between the updraft and environmental air is parameterized as the sum of two processes: the organized entrainment that characterizes large-scale mixing and the turbulent entrainment for small-scale mixing at the edge of the clouds. For deep convection, the organized entrainment is calculated using the vertically integrated updraft buoyancy, whereas the turbulent entrainment rate is set to 0.1 km^{-1}. The closure for deep convection is based on a quasi-equilibrium assumption, where the convective available potential energy (CAPE) is consumed over a

prescribed relaxation timescale. The trigger of convection is based on the buoyancy at the lifting condensation level, resulting from an updraft that is lifted dry adiabatically from the surface. An additional buoyancy is added based on the variance of potential temperature in the boundary layer to account for subgrid variability.

2.2. Description of Experiments

To explore how different components of the convection scheme affect the precipitation distribution, sensitivity experiments are performed using the standard ECHAM6 configuration in T63 with 47 levels in the vertical. The model is run using an Atmospheric Model Intercomparison Project style integration [*Taylor et al.*, 2000] with 1986–1991 observed SSTs [*Hurrell et al.*, 2008]. The first year is discarded as a spin-up period and only the last 5 years are used for the analysis. We perform two control simulations, one with the default Nordeng scheme (CTRL) and the other with the original Tiedtke scheme for deep convection (CTRL_Tiedtke). Six experiments are performed corresponding to changes to the trigger, cloud model, and closure for deep convection in the default Nordeng scheme, applied separately over land and over ocean. Modifications are imposed only during the months June-July-August (JJA), and the Nordeng scheme remains unchanged for the other months. This is done in order to focus on the interaction between the convection scheme and the boreal summer circulation and to exclude the influence of precipitation and circulation biases from other seasons.

Some of the changes applied to the Nordeng scheme are designed to mimic the original Tiedtke scheme for deep convection, which gives a better precipitation distribution over the tropical Atlantic (see next section). Due to a mistake in the computation of the cloud top height, the Tiedtke scheme produces higher cloud tops in drier atmospheres [*Moebis and Stevens*, 2012]. This means that convective updrafts are less sensitive to environmental air when the Tiedtke scheme in used. To mimic this behavior, we modify the Nordeng scheme in EXP_NoEntrainment such that the turbulent entrainment is set to zero. This results in less diluted updrafts, which in theory means an easier production of deep convection in the model. Tiedtke also differs from Nordeng in terms of the closure for deep convection. In EXP_ConvergenceClosure, the default CAPE closure in Nordeng is replaced by a closure based on moisture convergence in the boundary layer as used in the original Tiedtke scheme. Finally, we performed one additional experiment where we modified the trigger, in order to test all three components of the convection scheme. For consistency with the entrainment experiment, we modified the trigger so as to trigger convection more easily. This is done in the experiment EXP_EasyTrigger, by setting the buoyancy added to the test parcel to its maximum value of 1 K. The letters L and O at the end of the experiment name denote whether the convection scheme is modified only over land or over ocean, respectively.

As an observational reference, we use the Global Precipitation Climatology Project (GPCP) version 2 [*Adler et al.*, 2003]. The GPCP data set combines satellite and rain gauge measurements and covers the period 1979–2010 with a 2.5° spatial resolution.

3. The Convection Scheme

The observed and simulated summertime precipitation distributions are shown in Figures 1a and 1b. Comparing the two clearly shows how the model ECHAM6, with the default Nordeng scheme for deep convection, fails to capture important features of the observed precipitation distribution. Precipitation is overestimated in the west Atlantic, in stark contrast to the eastward ITCZ maximum in observations. Over land, the model suffers from deficient rainfall, especially over Amazon and West Africa, where precipitation is underestimated by at least 2 mm d^{-1}. That precipitation is overestimated over ocean and underestimated over land indicates that the two might be related problems. Interestingly, by using a different convection scheme, Tiedtke, the precipitation improves both over ocean and over land (Figure 1c). An eastward shift of the Atlantic ITCZ maximum occurs, accompanied by an increase in rainfall over land, especially over West Africa. The different precipitation distributions in Figures 1b and 1c provide an opportunity to test the impact of varying formulations of the convection scheme.

By modifying the convection scheme, we primarily change the distribution of convection, not its total amount. In all our simulations, the mean rainfall amount in the tropics remains approximately constant at 3.5 mm d^{-1}, except in EXP_NoEntrainment_L which has a mean rainfall rate of 3.7 mm d^{-1}. Tropical precipitation in our model is mostly convective.

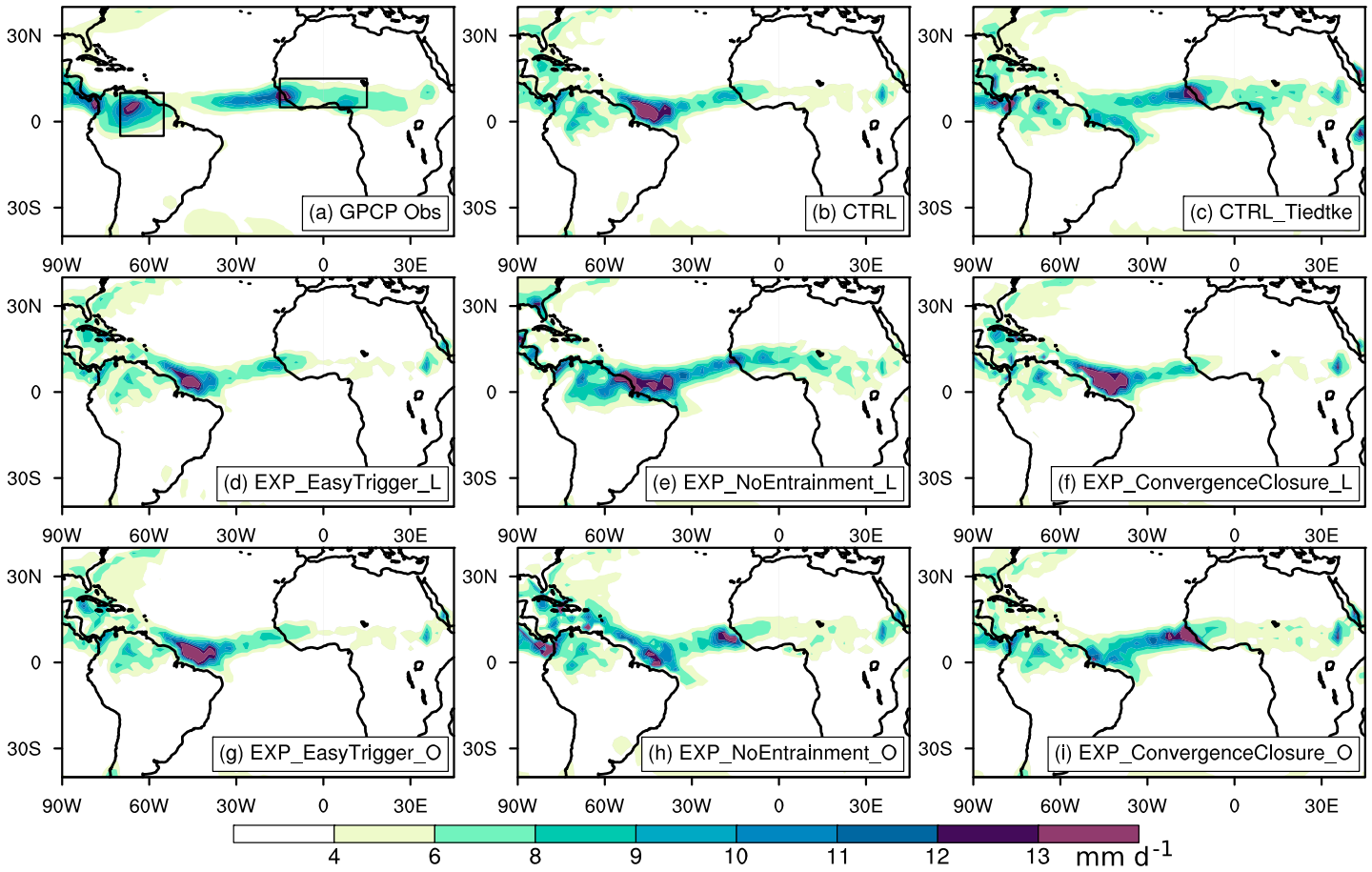

Figure 1. Mean state of boreal summer precipitation over the tropical Atlantic in (a) GPCP observations, (b) control simulation with the default Nordeng scheme (CTRL), (c) control simulation with the Tiedtke scheme (CTRL_Tiedtke), and (d–i) experiments with modified Nordeng scheme. The boxes in Figure 1a indicate the Amazon and West African regions where precipitation is averaged over in Figure 2.

3.1. Precipitation Biases Over Land

Figures 1d–1f show the precipitation distributions resulting from the applied changes to the trigger, entrainment, and closure over land, respectively. Among these, only turning off turbulent entrainment over land is able to affect the amount of rainfall over land. This is true for both Amazon and West Africa, as quantified in Figure 2. When turbulent entrainment is set to zero, the average precipitation over Amazon increases from 5.6 to 8.2 mm d^{-1}, whereas over West Africa, rainfall increases from 4.0 to 6.6 mm d^{-1}, close to the observed values. In contrast, modifications to the trigger and closure have no impact on the dry bias over land. The increase of 0.2 mm d^{-1} in the tropical mean precipitation in EXP_NoEntrainment_L is less than the obtained 0.9 mm d^{-1} increase over tropical land. This means that an increase over land would remain visible even if the model would be retuned to match the tropical mean precipitation in CTRL.

The entrainment rate sets the convective updraft's sensitivity to environmental air, and in particular to the free-tropospheric humidity. The higher the entrainment rate, the more diluted and hence less buoyant the updraft becomes. Removing turbulent entrainment in the experiment EXP_NoEntrainment_L, although unphysical, has the expected effect of increasing the fraction of convective events over land which reach high (≤250 hPa) cloud tops, as shown in Figure 3. The total number of triggered convective events is roughly the same for both cases. We choose 250 hPa as a measure for deep convection as it is found to adequately represent the spatial distribution of precipitation events >4 mm d^{-1}. Setting the turbulent entrainment to zero allows for more frequent deep clouds and, as a consequence, increases the rainfall amount and net convective heating over land. The increased precipitation also translates to a wetter atmosphere over land. Over the Sahel, for instance, EXP_NoEntrainment_L has a specific humidity profile that is in better agreement with observations from the Atmospheric Infrared Sounder [*Tian et al.*, 2013] climatology (not shown).

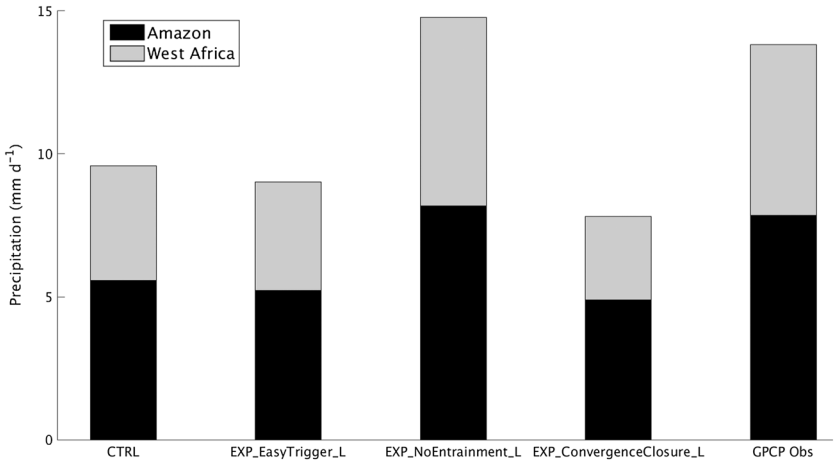

Figure 2. Area-averaged summer precipitation over northern Amazon (55°–70°W, 5°S–10°N) and West Africa (15°W–15°E, 5°–15°N) in CTRL, experiments with modified Nordeng scheme over land, and GPCP observations.

This indicates that the dry bias over land can be explained by convection that is not deep enough in the model, which is consistent with the lack of impact of the trigger and closure modifications. Even if the triggering of convection is artificially enhanced (EXP_EasyTrigger_L), or the strength of convection formulated differently (EXP_ConvergenceClosure_L), the resulting updrafts will be nonetheless suppressed by a high entrainment rate.

Prescribing a lower entrainment rate over land than over ocean has also been shown by *Zhao et al.* [2009] to result in a reduction of the dry precipitation bias over land in the Geophysical Fluid Dynamics Laboratory (GFDL) HIRAM2.1 model. By decreasing the land-to-ocean entrainment rate ratio, they found that precipitation over tropical land areas increases, especially over the Amazon region. The coarser the model horizontal resolution, the lower the land-to-ocean entrainment rate ratio should be.

Although the modification in EXP_NoEntrainment_L is unphysical, there is some basis behind the idea that entrainment rates must be lower over land than over ocean. Observational studies have shown that convection over land is stronger [*Zipser*, 2003] and deeper [*Liu and Zipser*, 2005] than over ocean. One possible explanation is the different updraft widths between land and ocean [*Lucas et al.*, 1994; *Williams and Stanfill*, 2002; *Zipser*, 2003]. Because entrainment rates are inversely proportional to the updraft width [*Turner*, 1963], the typically larger updraft widths over land means that there is less entrainment of environmental air over land.

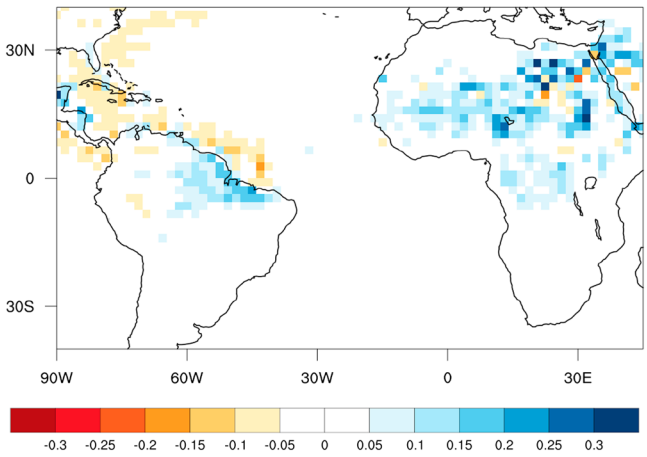

Figure 3. Difference in fraction of convective events (based on 6-hourly output) which reach cloud tops ≤250 hPa between EXP_NoEntrainment_L and CTRL.

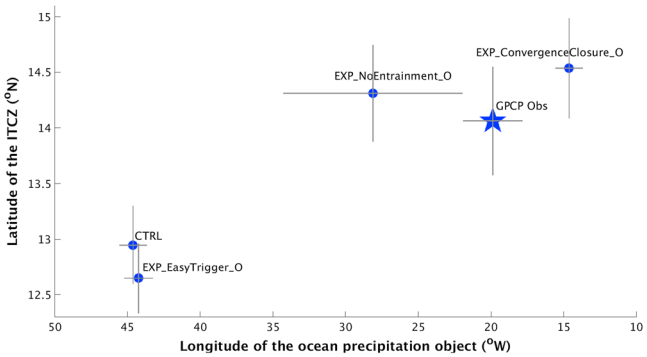

Figure 4. Longitude of the Atlantic ocean object plotted against the northernmost latitude of the Atlantic ITCZ (marked by the 2 mm d^{-1} contour at 25°W). The blue star marks the Atlantic ITCZ in GPCP observations. The gray bars show the standard error due to sampling uncertainty arising from the interannual variation in the longitudinal and latitudinal positions.

It is also possible that features necessary for the production of deep convection over land are either absent or misrepresented in the model, and removing turbulent entrainment merely compensates for such errors. For instance, GCMs struggle to represent African easterly waves [*Martin and Thorncroft*, 2015; *Skinner and Diffenbaugh*, 2013], which are synoptic-scale disturbances known for their role in organizing mesoscale convective systems in West Africa [*Carlson*, 1969; *Fink and Reiner*, 2003]. Moreover, mesoscale circulations due to surface heterogeneities, such as gradients in soil moisture, have been shown to be important for the generation of precipitation in the Sahel region and are known to be misrepresented in GCMs [*Taylor et al.*, 2011].

3.2. Precipitation Biases Over Ocean

In Figure 4, the Atlantic ITCZ is evaluated in terms of its northernmost latitude, marked by the 2 mm d^{-1} contour at 25°W, and its longitude, marked by the centroid of the ocean precipitation object. The ocean precipitation object is defined here as the largest contiguous area with precipitation values greater than 70% of the maximum precipitation over ocean [*Wernli et al.*, 2008; *Hohenegger and Stevens*, 2013; *Siongco et al.*, 2015]. The latitude of the Atlantic ITCZ is measured at the central Atlantic at 25°W, in consideration of its tilted east-west structure. Figure 4 shows the westward and southward ITCZ location in the control simulation, in contrast to the eastward and northward ITCZ in observations. Enhancing the convective trigger over ocean (EXP_EasyTrigger_O) does little to improve the erroneous Atlantic ITCZ in the control. This is because over ocean, convection is anyway triggered frequently due to the unlimited moisture supply. In the experiment without turbulent entrainment over ocean (EXP_NoEntrainment_O), the Atlantic ITCZ shifts northward and eastward, in better agreement with observations, but with a relatively large variability in its longitudinal position. Comparing Figures 1b and 1h, we see that from a single cluster of westward rainfall maximum in CTRL, two peaks develop over the west and over the east Atlantic coasts in the simulation with turbulent entrainment off. The precipitation object fluctuates between the two maxima from year to year, leading to the large variability in the longitudinal location of the ocean object in EXP_NoEntrainment_O. In contrast, EXP_ConvergenceClosure_O shows a distinct eastward ITCZ maximum (Figure 1i) that reproduces the observed longitudinal ITCZ position (Figure 1a), although the maximum is now 5° too far east. At the same time, the ITCZ is now located 1.5° north from the observations (Figure 4). It is by switching to a moisture convergence closure that the simulated Atlantic ITCZ shifts toward its most northward and most eastward position.

With a CAPE closure, the mass flux at cloud base is strongly coupled to the underlying SST, whereas with a moisture convergence closure, convection is decoupled from SST (Figure 5). This explains why in the former, the ITCZ maximum is found at the west Atlantic, while in the latter, precipitation peaks elsewhere. *Song and Zhang* [2009] also found that a convection scheme with a CAPE closure tends to collocate precipitation and SST too strongly, whereas one with a non-CAPE closure is less sensitive to SSTs and has a more realistic ITCZ over the Pacific. Because free-tropospheric temperatures in the tropics tend to be horizontally uniform [*Sobel and Bretherton*, 2000], the use of a CAPE closure is, by design, tantamount to a strong sensitivity to SSTs.

The decreased sensitivity to SSTs in EXP_ConvergenceClosure_O gives way to an increased sensitivity to the monsoon circulation in the eastern part of the domain. Figure 6a shows the zonal wind averaged over the east Atlantic region (15°–30°W). In CTRL (black line), we see a background easterly flow that gets weaker as

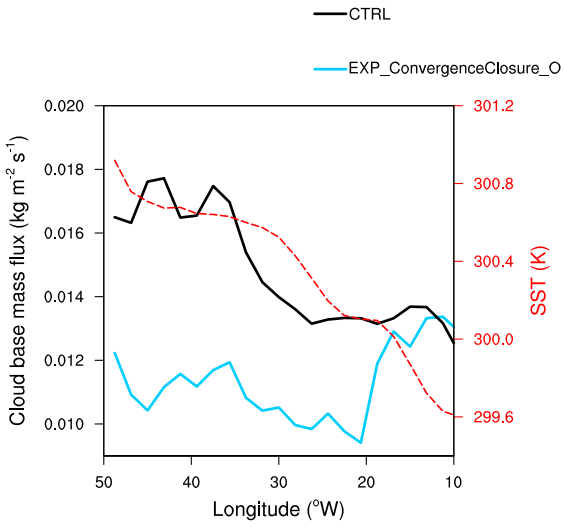

Figure 5. Longitudinal intensity profile of the cloud base mass flux averaged over 5°S–15°N for the control (black line) and experiment with moisture convergence closure over ocean (blue line). The red line shows the prescribed SST.

the latitude increases, due to the westerly monsoon flow into West Africa. While EXP_ConvergenceClosure_O (blue line) has a similar shape, its profile is shifted to the right, to weaker easterlies. Compared to CTRL, EXP_ConvergenceClosure_O has a stronger westerly monsoon flow, peaking at 7.5°N (Figure 6b). With a closure based on moisture convergence, it can explicitly detect the convergence associated with the West African monsoon and starts raining at the east Atlantic. Rain on the east Atlantic increases convergence, which enhances the monsoonal flow. This results in increased moisture convergence, sustaining a positive feedback that decisively shifts the precipitation maximum toward the east Atlantic (Figure 1i). In contrast, with a closure based on CAPE, excessive precipitation over warm SSTs in the west Atlantic weakens convergence at the east Atlantic and disrupts the monsoonal flow. That errors in the strength or location of convection can alter the background flow has been found in other studies, both in idealized [*Hohenegger et al.*, 2015] and in more realistic simulations [*Marsham et al.*, 2013].

A positive feedback with the monsoon flow is notably absent in EXP_NoEntrainment_O, as shown by the purple line in Figure 6b. Its lack of latitudinal dependence is instead indicative of an overall weakening of the easterly flow, induced by the precipitation maximum that emerges at the east coast when turbulent entrainment is turned off. Why does a second rainfall maximum develop at the east Atlantic when turbulent entrainment is turned off? In the control simulation with turbulent entrainment, precipitation exhibits a tight coupling with the humidity at 850 hPa (Figure 7). The precipitation maximizes at the west Atlantic, where the lower free troposphere is moist, whereas a precipitation minimum occurs at the east Atlantic, where it is dry. Turning off entrainment weakens this coupling by decreasing the sensitivity of convection to free-tropospheric humidity: it can rain anywhere, even in regions where it is dry. This is consistent with the dashed black curve in Figure 7, which shows an increase in rainfall in the east Atlantic. The proximity of the east Atlantic to the dry Sahara makes the entrainment rate especially important in this region. In addition to the zonal response, the Atlantic ITCZ also broadens meridionally when turbulent entrainment is off (Figure 1h),

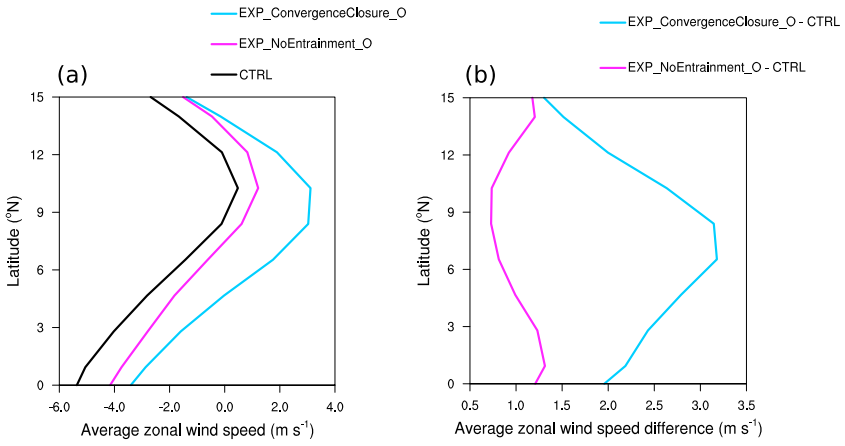

Figure 6. (a) The zonal wind averaged over 15°–30°W plotted against latitude and (b) the difference with respect to CTRL for the two experiments EXP_NoEntrainment_O and EXP_ConvergenceClosure_O.

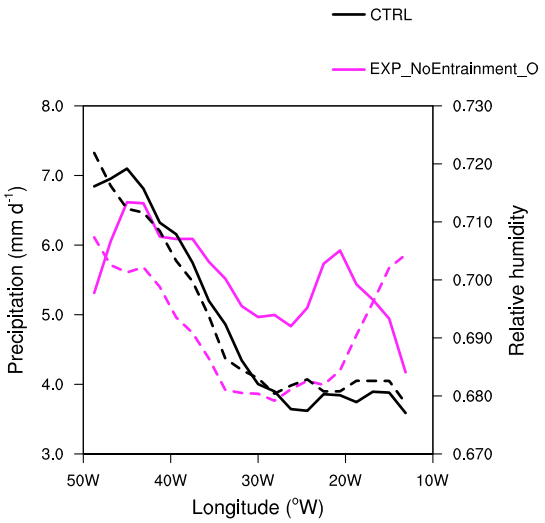

Figure 7. Longitudinal intensity profile of precipitation (solid lines) averaged over 5°S–15°N for the control (black) and experiment with no turbulent entrainment over ocean (purple). The dashed lines show the relative humidity at 850 hPa.

reminiscent of a double ITCZ response to weakened entrainment rates seen in aqua-planet setups [*Moebis and Stevens*, 2012; *Oueslati and Bellon*, 2013].

Although convection is enhanced over the east Atlantic in EXP_NoEntrainment_O, its CAPE-based closure still implies that convection is, at the same time, favored over the warm SSTs at the west Atlantic. This explains the persistence of the westward Atlantic ITCZ bias in EXP_NoEntrainment_O (Figures 1h and 4). A complete shift of the ITCZ maximum toward the east Atlantic is only possible with a moisture convergence-based closure, which outweighs the oversensitivity to SST in the west Atlantic.

3.3. Interaction of Land-Ocean Biases

Changes to the convection scheme applied separately for land and ocean also give us an opportunity to understand how land affects the Atlantic ITCZ and vice versa. Specifically, we test whether an improved simulation of the Atlantic ITCZ alters the large-scale circulation so as to overcome the dry bias over land and whether increasing precipitation over land can shift the position of the Atlantic ITCZ.

In simulations with modifications applied over ocean (Figures 1g–1i), the dry bias over land areas persists. Precipitation over the Amazon in all three cases does not differ from the control (Figure 1b) and remains underestimated compared to observations (Figure 1a). Over West Africa (15°W–15°E, 5°–15°N), precipitation values in EXP_NoEntrainment_O (4.9 mm d^{-1}) and EXP_ConvergenceClosure_O (5.1 mm d^{-1}) are higher than in EXP_EasyTrigger_O (3.8 mm d^{-1}) and CTRL (4.0 mm d^{-1}). This is likely due to the fact that in both Figures 1h and 1i, an ITCZ maximum develops in the eastern Atlantic. The eastward ITCZ maximum enhances low-level wind convergence over West Africa, either by an overall weakening of the easterly flow (EXP_NoEntrainment_O) or by a strengthening of the westerly monsoon flow (EXP_ConvergenceClosure_O) (see Figure 6b). Nevertheless, in both cases, the West African rainfall remains lower compared to the case where entrainment is turned off over land (6.6 mm d^{-1}). This means that the dry bias over land is only weakly influenced by the Atlantic ITCZ.

In simulations with modifications applied over land (Figures 1d–1f), the Atlantic ITCZ bias persists. All have excessive precipitation at the west Atlantic and a southward ITCZ position, similar to biases in the control simulation. The increased precipitation over land in EXP_NoEntrainment_L decreases the mean precipitation over tropical ocean, resulting in a more realistic land-to-ocean precipitation ratio over the tropics. Despite this, EXP_NoEntrainment_L still exhibits an erroneous Atlantic ITCZ position (Figure 1e).

That the biases over land and the biases over ocean only have minimal influence on each other highlight the fact that these are two separate issues. Over land, the shortcoming is in the amount of rainfall, because convection is not deep enough. Over ocean, the bias is in the position of the simulated ITCZ, because convection is not sensitive enough to the monsoon circulation in the east Atlantic. Although their experimental framework is different, *Biasutti et al.* [2004] arrived at similar conclusions regarding the interaction between precipitation over land and precipitation over ocean in the tropical Atlantic. Using the CCM3 model, they first showed that the simulated continental precipitation is controlled by insolation, whereas the simulated oceanic precipitation strongly follows SST. By varying SSTs and fixing insolation, they find that oceanic convection does not have a strong impact on continental precipitation, except in coastal regions. In another experiment, with fixed SSTs and varying insolation, their results show that precipitation over land can influence the amount of precipitation over ocean but not the ITCZ position.

4. The Horizontal Resolution

The previous results have shown how precipitation biases over land and over ocean in the tropical Atlantic are affected by the parameterization of convection in a given grid box. Our next step is to look at the influence of the grid box size itself. In this section, we investigate the role of horizontal resolution on the tropical Atlantic precipitation distribution. Specifically, we test the sensitivity of the biases to the resolution of the atmosphere (A), orography (O), and land surface (S). To isolate their relative contributions, we apply a factor separation analysis [*Stein and Alpert*, 1993], which requires that we selectively activate each of the three factors. This is implemented through the sensitivity experiments described in section 4.1.

4.1. Description of Experiments

Sensitivity experiments are performed using ECHAM6.2 in T255 with 95 levels in the vertical. Hereafter, we use the naming convention $F_{A/O/S}$, with the subscript denoting the operating factor in each simulation. For example, F_A is a simulation with only the atmosphere in high resolution, whereas the surface and orography are in low resolution. $\hat{F}_{A/O/S}$ denotes the relative contribution to the precipitation field by the operating factor. Details of how the contribution terms $\hat{F}_{A/O/S}$ are calculated are given in the Appendix.

From the necessary simulations, only F_{AOS}, F_{AS}, F_{AO}, F_A, and F_{off} can be performed. For the simulation with all factors off (F_{off}), we use the control simulation in T63 from the previous section. The simulations F_{OS}, F_O, and F_S require a low resolution atmosphere with a high-resolution orography and/or surface, which is not feasible. This means that for the orography and surface factors, their individual contributions to the precipitation field cannot be decomposed fully, resulting in residual terms. We can, however, completely isolate the contribution of the atmosphere factor (see Appendix).

The high-resolution orography factor is turned off by running the model at T255 with T63 orography. We truncate the geopotential to T63 by setting the higher wave numbers to zero. The orographic fields used in the subgrid orography scheme are also replaced with their T63 counterparts. Similarly, the high-resolution surface factor is turned off by running the model at T255 with T63 land surface parameters. Among these parameters are land-sea mask, surface albedo, leaf area index, and soil moisture. Due to the high computational cost, these simulations are only run for 1 year with prescribed 1988 SSTs. All simulations use 95 vertical levels except F_{off}. Since the precipitation distribution in F_{off} is similar to a simulation with 95 levels, the different vertical resolution in F_{off} does not have an impact on our results.

4.2. Relative Roles of a High-Resolution Atmosphere, Orography, and Surface

Figure 8 shows the precipitation distribution in the simulation F_{AOS} and the difference compared to F_{off}. Over land, we see that the amount of rainfall increases as resolution increases, especially over orographic regions like the northern Andes. The average rainfall amounts over Amazon and West Africa are 6.5 mm d^{-1} and 4.0 mm d^{-1}, respectively. These values, however, differ little from corresponding amounts in the CTRL (5.6 and 4.0 mm d^{-1}) and are still below the observations (7.9 and 6.0 mm d^{-1}), showing that the dry bias over land in the tropical Atlantic cannot be removed by increasing resolution alone. In contrast, over ocean, increasing the resolution results in a major improvement of the Atlantic ITCZ position, which shifts northward (13.6°N) and eastward (20.6°E), closer to the observations.

Although F_{AOS} is run for only 1 year, its eastward Atlantic ITCZ maximum is comparable to a 30 year integration of ECHAM6 in T255 (not shown). In fact, the resolution dependence of the Atlantic ITCZ position in F_{AOS} is also evident in other AGCMs. High-resolution models like Meteorological Research Institute-AGCM, MIROC5, and GFDL-HIRAM-C180 all have an eastward ITCZ maximum, whereas low-resolution models have a tendency to misplace it westward [*Siongco et al.*, 2015].

To better understand why F_{AOS} rains more over the east Atlantic than F_{off}, we use the factor separation approach discussed in the beginning of this section. The relative contributions of a high-resolution orography, atmosphere, and surface are shown in Figure 9. With a high-resolution orography, the precipitation response is dominated by the enhanced convection at the east Atlantic. There is also more precipitation over the continents, especially near orographic regions, and a weak decrease at the west Atlantic (Figure 9a). With a high-resolution atmosphere, enhanced convection occurs starting at East Africa and continues up to the West African coast. Further downstream, at the coast of Brazil, there is a substantial decrease in precipitation of more than 5 mm d^{-1} at the west Atlantic (Figure 9b). In contrast to the orographic and atmospheric responses, the effect of a high-resolution land surface is minimal (Figure 9c). While the resolution of land

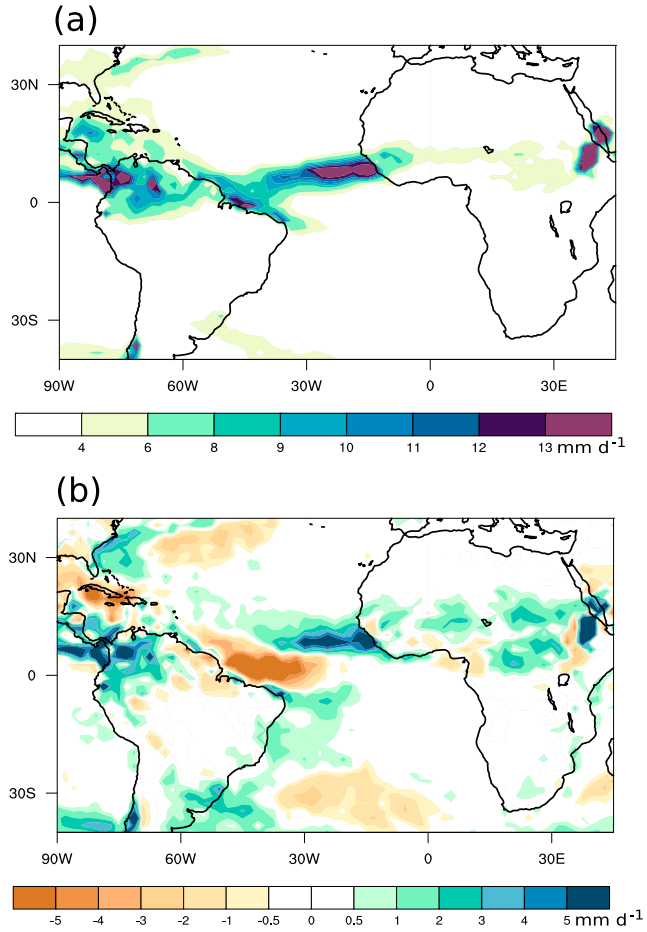

Figure 8. Summer precipitation in (a) F_{AOS} and the difference (b) $F_{AOS} - F_{off}$.

surface fields such as land-sea mask is certainly crucial over regions like the Maritime Continent [*Schiemann et al.*, 2013], it is apparently not as important over larger landmasses like South America or Africa. We thus interpret the improved Atlantic ITCZ in Figure 8 as the sum of two main contributions: the orographic effect (Figure 9a) and the atmospheric effect (Figure 9b).

4.2.1. The Effect of a High-Resolution Orography

Although high-resolution orography is imposed everywhere, our hypothesis is that the precipitation change in Figure 9a is a response to better resolved orography over South America and Africa in particular. Additional experiments, where orography is smoothed only over South America ($F_{AO_{[SAm]S}}$) or only over Africa ($F_{AO_{[Afr]S}}$), are used to test this hypothesis. The selective smoothing of orography is achieved by first converting the T63 and T255 spectral orography into grid point space and then applying a mask to replace the T255 orography with its T63 counterpart, but only over the area of interest ([SAm], [Afr]). The modified T255 orography is converted back into spectral space and prescribed into the model.

The effect of a high-resolution orography over South America during boreal summer is shown in Figure 10a. With high-resolution orography over South America, the mean easterly flow becomes weaker (apparent westerly flow) along the equator, accompanied by precipitation decrease in the west Atlantic and increase in the east Atlantic. Since the Andes are the most prominent orographic feature over South America, we attribute most of these changes to the Andes. *Xu et al.* [2004] pointed out that resolution is especially important in the northern portion of the Andes, where the mountains cover only about 200 km and would be hardly resolved by a low-resolution model. They found that with a high-resolution Andes, there is more blocking and hence a weaker mean easterly flow, which reduces the anomalous precipitation in the eastern Pacific. A similar effect occurs in Figure 10a, but with the impact over the Atlantic. The weaker mean easterly flow induced by the better resolved Andes suppresses convection in the west Atlantic, which sustains the enhanced convection

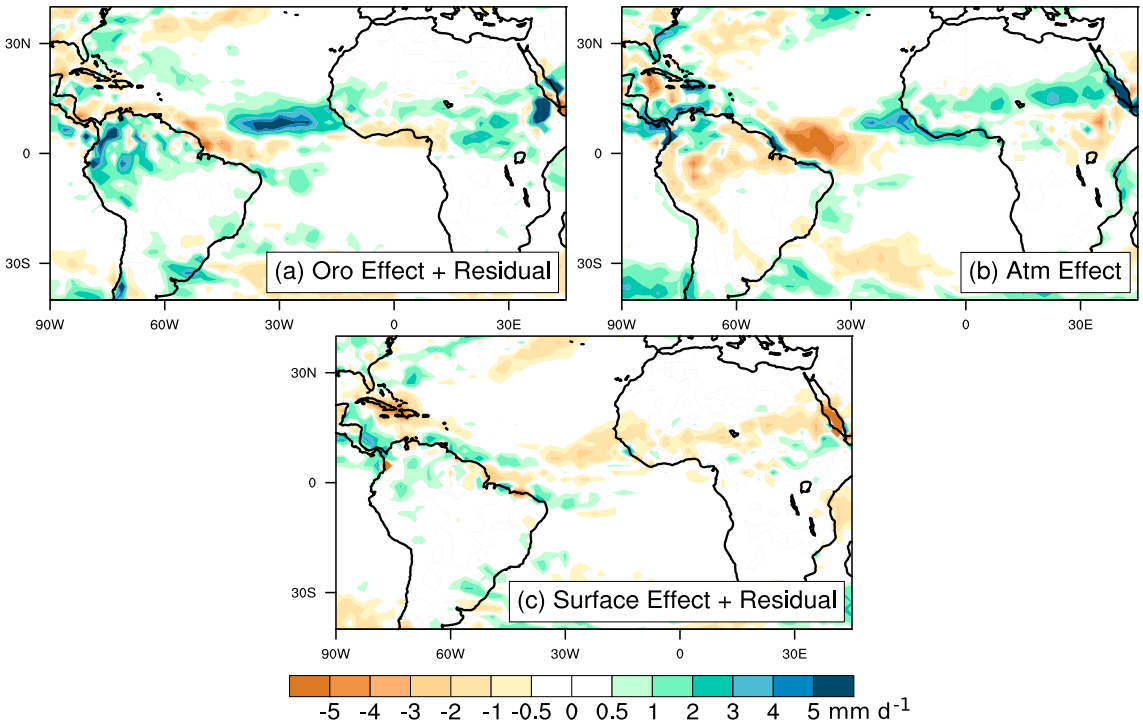

Figure 9. Factor-separated summer precipitation contribution from a high-resolution (a) orography ($\hat{F}_O$) + residual terms ($\hat{F}_{AO} + \hat{F}_{OS} + \hat{F}_{AOS}$), (b) atmosphere ($\hat{F}_A$), and (c) surface ($\hat{F}_S$) + residual term with atmosphere ($\hat{F}_{AS}$). The calculations of the contribution terms are given in the Appendix.

in the east Atlantic. In absence of a direct relationship with the monsoon flow, the orographic effect of the Andes on the circulation shows little latitudinal dependence (dashed line in Figure 10c) from the equator until 8°N. As the Andes vanish north of 8°N, the orographic effect also weakens.

The effect of a high-resolution orography over Africa is shown in Figure 10b. With better resolved African orography, a cyclonic circulation becomes apparent, together with an increase in rainfall over the eastern Atlantic. Note that this increase is further northward as compared to that of Figure 10a, following the northward tilt of cyclonic pattern. *Semazzi and Sun* [1997] proposed an explanation for the orographically induced cyclonic circulation in the east Atlantic. By performing simulations with and without African topography, they showed that the presence of the Atlas-Ahaggar mountains in north Africa creates a windward high-pressure and leeward low-pressure distribution. The leeward low pressure interacts with the westerly monsoon flow and generates a cyclonic circulation near the coast of West Africa. This enhances moisture convergence and convection in the east Atlantic. With high-resolution orography over Africa, we expect that such orography-monsoon interactions become more intensified, resulting in the enhanced cyclonic circulation and increased east Atlantic precipitation in Figure 10b. In contrast to the Andes, the effect of African orography increases with latitude, starting from 5°N and peaking at 14°N (dotted line in Figure 10c).

The full effect of a high-resolution orography is shown by the solid line in Figure 10c. From 0 to 8°N, the South American orography has the bigger contribution to the magnitude of the full orographic response. However, the latitudinal increase in the full orographic response from 5 to 8°N is shaped by the African orography, as the contribution from the South American orography remains meridionally constant. From 8°N northward, the effect of the South American orography weakens, gradually at first, and then sharply north of 12°N. Meanwhile, the effect of the African orography continues to strengthen with latitude, compensating for the weakening of the South American effect north of 12°N. This is consistent with the precipitation responses in Figures 10a and 10b: the precipitation increase from the African orography is more northward than its South American counterpart.

Analogous to the closure effect in Figure 6b, it is the interaction of better resolved orography over Africa with the westerly monsoon flow which gives the latitudinal dependence to the profile. Similarly, the lack of a direct relationship with the monsoon from better resolved South American orography is reflected in the uniform

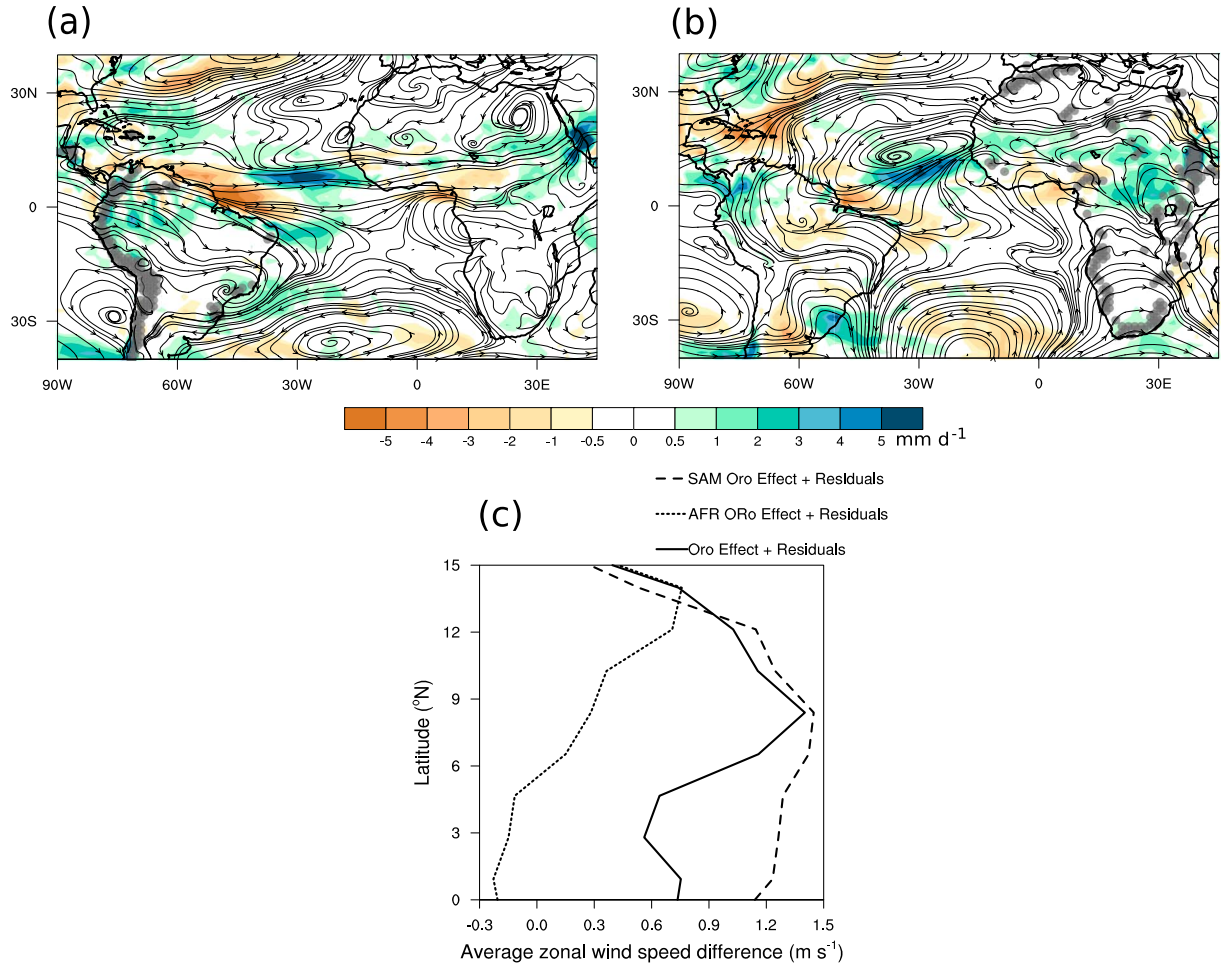

Figure 10. Difference in horizontal streamline wind pattern at 850 hPa and precipitation of (a) $F_{AOS} - F_{AO_{[SAm]}S}$ (contribution from high-resolution orography over South America), (b) $F_{AOS} - F_{AO_{[Afr]}S}$ (contribution from high-resolution orography over Africa), and (c) the zonal wind difference, averaged across 15° – 30°W and plotted against latitude. The gray shadings in Figures 10a and 10b show the regions of differences in orography with respect to F_{AOS} for the experiments $F_{AO_{[SAm]}S}$ and $F_{AO_{[Afr]}S\sqrt{i}}$.

weakening of easterlies, akin to the entrainment effect in Figure 6b. There is, however, an important distinction between Figures 6b and 10c. The closure and entrainment effects change the behavior of convection, to which the circulation responds. The orographic effects from both Africa and South America directly change the circulation, to which convection responds.

A comparison of the magnitude of the full orographic effect in Figure 10c with the closure effect in Figure 6b shows that while a positive feedback with the monsoon flow is evident in both, the orographic effect is overall much weaker than the closure effect. This emphasizes the fact that although there is higher-resolution orography everywhere, the use of a CAPE closure would still consistently favor rain over the west Atlantic and act against the monsoon flow.

4.2.2. The Effect of a High-Resolution Atmosphere

The precipitation response to a change in the resolution of the atmospheric grid (Figure 9b) brings us back to the role of convective parameterization. With a high-resolution atmosphere, certain aspects of the parameterized convection change. We focus on two possible resolution-dependent behaviors. First, as resolution increases, it becomes easier to trigger convection since saturation levels are reached more quickly with a smaller grid box size. Second, the resolved magnitude of the vertical velocity increases as the grid size is reduced. This is why in ECHAM6, with the default Nordeng scheme, the relaxation timescale for CAPE removal is set to decrease fourfold (i.e., mass flux at cloud base increases fourfold) as we go from a T63 to a T255 atmospheric grid (e.g., from F_{off} to F_A). The smaller adjustment timescale prevents the explicit convection

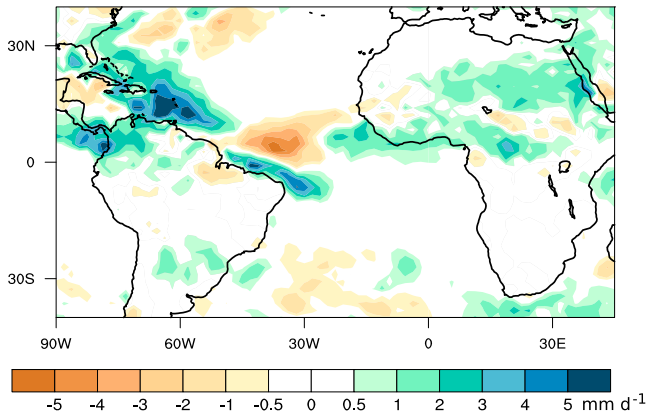

Figure 11. Summer precipitation difference between EXP_StrongerMassFlux and CTRL.

from taking over by making the convection scheme more active [*Done et al.*, 2006]. This means that as we go from a T63 to a T255 atmospheric grid, the fraction of stratiform to convective precipitation over the tropical Atlantic remains approximately the same (from 0.31 to 0.34), and precipitation in both cases comes mostly from the convective component. The question then is which of the two possible effects, the easier trigger or the stronger cloud base mass flux, can explain Figure 9b.

A simple way to test the two hypotheses is to mimic the atmospheric resolution effect in low resolution by modifying the trigger and the closure. In fact, the EXP_EasyTrigger simulations from section 3 have already addressed our first hypothesis. If the atmospheric resolution effect comes from the easier triggering of convection, artificially making it easier to rain in low resolution should be able to replicate the precipitation response in Figure 9b. However, as we have shown previously, the Atlantic ITCZ responds weakly to the modified trigger (see Figures 1d and 1g), hence disproving our first hypothesis.

To test the second hypothesis, we modify the Nordeng scheme such that the cloud base mass flux is increased by four times (EXP_StrongerMassFlux). The result is shown in Figure 11. Comparing Figure 11 to Figure 9b, we see that the effect of a stronger cloud base mass flux on the precipitation distribution is similar to that of a high-resolution atmosphere. Figure 9b can thus be interpreted as the consequence of a resolution-dependent closure. The tendency of convection to occur more strongly makes it easier to rain in the model, which pushes convection in what would otherwise be less favorable conditions upstream in the east Atlantic. Increased convection upstream weakens the easterly flow and reduces precipitation downstream in the west Atlantic. The weaker easterly flow in EXP_StrongerMassFlux with respect to CTRL is shown as the dashed line in Figure 12. It has a comparable profile to that of the atmospheric effect $\hat{F}_A$ (solid line), further confirming our finding that the effect of a high-resolution atmosphere can be explained as a mass flux effect. Both effects are in fact similar to the entrainment effect in section 3 (see Figure 6b).

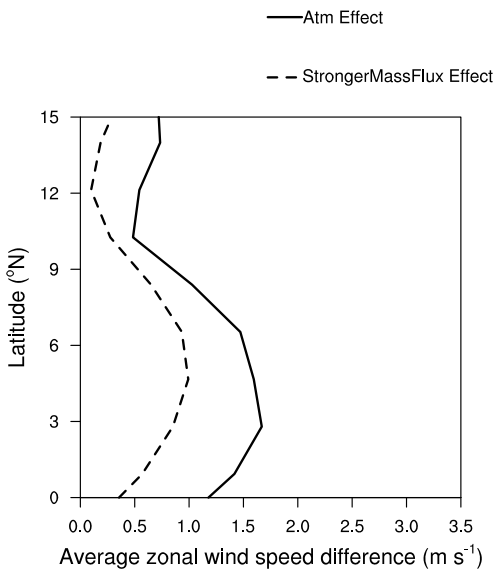

Figure 12. The zonal wind difference from CTRL, averaged over 15°–30°W and plotted against latitude in EXP_StrongerMassFlux (dashed line) and in the factor-separated atmospheric effect $\hat{F}_A$ (solid line).

5. Conclusions

During boreal summer, the observed Atlantic ITCZ shifts northward and eastward toward West Africa, in accordance with the onset of the monsoon. The model ECHAM6 fails to capture such a shift, as the simulated Atlantic ITCZ remains westward and southward near the coast of Brazil. The erroneous

Atlantic ITCZ position is accompanied by deficient rainfall over land areas, especially over Amazon and West Africa. These problems are common to other AGCMs, but to differing degrees. In this study, reasons behind the dry bias over land and the incorrect Atlantic ITCZ position over ocean in the model ECHAM6 were explored. We first investigated how different components of a convection scheme impact the simulated precipitation distribution in the tropical Atlantic. Sensitivity experiments with modifications to the trigger, entrainment, and closure were performed. The modifications were applied separately over land and over ocean, which allowed us to study the relative importance of, and interaction between, the Atlantic ITCZ bias over ocean and the dry bias over land. Next, we explored how horizontal resolution impacts the biases through sensitivity experiments designed to infer the relative contributions from a high-resolution atmosphere, orography, and surface.

Our results showed that over land, the amount of precipitation is largely determined by the effectiveness with which a dry environment can act to suppress convection, which in ECHAM6 is mostly controlled by the specified entrainment rate. A high entrainment rate prevents convective updrafts from reaching high cloud tops and decreases the total amount of precipitation by as much as 2.6 mm d^{-1} over Amazon and West Africa.

Over ocean, we found that the Atlantic ITCZ position is determined by a tug-of-war between the propensity for convection in the west and in the east Atlantic. On one hand, the SSTs are warmer and the free troposphere is moister over the west Atlantic. On the other hand, the large-scale circulation, through the West African monsoon flow, works in favor of convection in the east Atlantic. Which of the two succeeds depends on the model design. The default Nordeng scheme in ECHAM6 produces an erroneous ITCZ maximum over the west Atlantic. In this work, we have identified three ways through which we can increase precipitation over the east Atlantic:

1. Make convection more sensitive to the circulation, in particular to the monsoon circulation in the east Atlantic. The type of closure we implement, whether it is based on moisture convergence or based on CAPE, sets the sensitivity of convection to the large-scale circulation.
2. Change the circulation directly. By modifying the resolution of the orography, we can change the strength of its impact on the large-scale circulation. A better resolved Andes weakens the easterly flow, whereas a better resolved orography over Africa strengthens the monsoon circulation. The combined effect leads to an enhancement of convection in the east Atlantic and a suppression in the west Atlantic.
3. Make it easier to rain in the model without directly changing the large-scale circulation. This can be achieved either by removing turbulent entrainment or by increasing the resolution of atmospheric grid. The tendency of convection to occur more easily enhances convection upstream in the east Atlantic, which then weakens the easterly flow and reduces convection in the west Atlantic.

Since biases over land and over ocean do not seem to interact, at least over the Atlantic, using different parameters in the convection scheme for land and ocean conditions might be defendable, although physically not fully satisfactory.

With a different season and set of large-scale conditions, convection in the model may be sensitive to other aspects of the parameterization and resolution. In boreal spring, for instance, the absence of a monsoon makes it less obvious why regions of warm SST would differ from regions of enhanced low-level convergence. As such, there is also no assurance that a convergence-sensitive closure will have a better precipitation distribution than an SST-sensitive one. In austral summer, continental heating is concentrated through much of South America and parts of South Africa. Other circulation features, such as the South Atlantic High and its interaction with the Andes, become more prominent [*Lenters and Cook*, 1995; *Rodwell and Hoskins*, 2001]. How well our GCMs represent the precipitation distribution, in different seasons and different regions, ultimately rests on our basic understanding of how convection couples with the large-scale circulation and of how this coupling adapts to seasonally and geographically varying conditions.

Appendix A: Factor Separation

The factor separation analysis of *Stein and Alpert* [1993] is applied for the case of the three factors: a high-resolution atmosphere (A), a high-resolution orography (O), and a high-resolution land surface (S). The precipitation field from a simulation with all factors active, F_{AOS}, can be decomposed as in equation (A1).

It is equal to the sum of the precipitation field when all the factors are turned off (F_{off}), plus the contributions due to each factor ($\hat{F}_A$, $\hat{F}_O$, $\hat{F}_S$), and the contributions due to the interaction of the factors (e.g., $\hat{F}_{AS}$).

$$F_{AOS} = F_{off} + \hat{F}_A + \hat{F}_O + \hat{F}_S + \hat{F}_{AS} + \hat{F}_{OS} + \hat{F}_{AO} + \hat{F}_{AOS} \tag{A1}$$

To isolate all the relative contribution terms ($\hat{F}$s), eight simulations are required: F_A, F_O, F_S, F_{AS}, F_{OS}, F_{AO}, F_{AOS}, and F_{off}. The individual contribution of each factor, for instance, orography is given by

$$\hat{F}_O = F_O - F_{off} \tag{A2}$$

The contribution due to the interaction terms, for instance, that of a high-resolution atmosphere and surface is given by

$$\hat{F}_{AS} = F_{AS} - (F_A + F_S) + F_{off} \tag{A3}$$

Equations (A2) and (A3) can be applied to the other factors and combinations thereof in order to complete the set of eight equations needed to resolve all the terms with $\hat{F}$.

However, as discussed in section 4.1, only five (F_{AOS}, F_{AS}, F_{AO}, F_A, F_{off}) out of the eight required simulations are performed. Hence, we only obtain the following five equations:

$$F_{AOS} - F_{off} = \hat{F}_A + \hat{F}_O + \hat{F}_S + \hat{F}_{AS} + \hat{F}_{AO} + \hat{F}_{OS} + \hat{F}_{AOS} \tag{A4}$$

$$F_A - F_{off} = \hat{F}_A \tag{A5}$$

$$F_{AOS} - F_{AS} = \hat{F}_O + \hat{F}_{AO} + \hat{F}_{OS} + \hat{F}_{AOS} \tag{A6}$$

$$F_{AOS} - F_{AO} = \hat{F}_S + \hat{F}_{AS} + \hat{F}_{OS} + \hat{F}_{AOS} \tag{A7}$$

$$F_{AOS} - F_A = \hat{F}_O + \hat{F}_S + \hat{F}_{AS} + \hat{F}_{AO} + \hat{F}_{OS} + \hat{F}_{AOS} \tag{A8}$$

Equation (A5) gives the fully isolated contribution from the atmosphere. In contrast, the orography and surface contributions include interaction terms (equations (A6) and (A7)). Subtracting equation (A6) from equation(A8), we get

$$F_{AS} - F_A = \hat{F}_S + \hat{F}_{AS} \tag{A9}$$

Doing so allows us to decompose equation (A4) into contributions from the atmosphere (equation (A5)), orography (equation (A6)), and surface (equation (A9)).

Acknowledgments
We thank Traute Crüeger and the two anonymous reviewers for their constructive comments and suggestions that helped to improve this manuscript. The research presented here was conducted while the corresponding author was employed by the Max Planck Institute for Meteorology. Primary data and scripts used in the analysis and other supporting information that may be useful in reproducing the author's work are archived by the Max Planck Institute for Meteorology and can be obtained by contacting publications@mpimet.mpg.de. The final stages of writing was performed under the auspices of the U.S. Department of Energy by Lawrence Livermore National Laboratory under contract DE-AC52-07NA27344.

References

Adler, R., et al. (2003), The version 2 Global Precipitation Climatology PGPCP) monthly precipitation analysis (1979–present), *J. Hydrometeorol.*, *4*, 1147–1167.
Biasutti, M., D. Battisti, and E. Sarachik (2004), Mechanisms controlling the annual cycle of precipitation in the Tropical Atlantic sector in an atmospheric GCM, *J. Clim.*, *17*, 4708–4723.
Biasutti, M., A. Sobel, and Y. Kushnir (2006), AGCM precipitation biases in the Tropical Atlantic, *J. Clim.*, *19*, 935–957.
Carlson, T. (1969), Synoptic histories of three African disturbances that developed into Atlantic hurricanes, *Mon. Weather Rev.*, *97*(3), 256–276, doi:10.1175/1520-0493(1969)097<0256:SHOTAD>2.3.CO;2.
Chao, W., and B. Chen (2004), Single and double ITCZ in an aquaplanet model with constant sea surface temperature and solar angle, *Clim. Dyn.*, *22*, 447–459.
Cook, K., and E. Vizy (2006), Coupled model simulations of the West African monsoon system: Twentieth- and twenty-first century simulations, *J. Clim.*, *19*, 3681–3703.
Davey, M., et al. (2002), STOIC: A study of coupled model climatology and variability in the tropical ocean regions, *Clim. Dyn.*, *18*, 403–420.
Done, J., G. Craig, S. Gray, P. Clark, and M. Gray (2006), Mesoscale simulations of organized convection: Importance of convective equilibrium, *Q. J. R. Meteorol. Soc.*, *132*, 737–756.
Duffy, P. B., B. Govindasamy, J. P. Iorio, J. Milovich, K. R. Sperber, K. E. Taylor, M. F. Wehner, and S. L. Thompson (2003), High-resolution simulations of global climate, Part 1: Present climate, *Clim. Dyn.*, *21*, 371–390.
Fink, A., and A. Reiner (2003), Spatiotemporal variability of the relation between African easterly waves and West African squall Lines in 1998 and 1999, *J. Geophys. Res.*, *108*(D11), 4332, doi:10.1029/2002JD002816.
Hohenegger, C., and B. Stevens (2013), Controls on and impacts of the diurnal cycle of deep convective precipitation, *J. Adv. Model. Earth Syst.*, *4*, 801–815, doi:10.1002/2012MS000216.
Hohenegger, C., L. Schlemmer, and L. Silvers (2015), Coupling of convection and circulation at various resolutions, *Tellus*, *67*, 26678.
Hourdin, F., et al. (2009), AMMA-model intercomparison project, *Bull. Am. Meteorol. Soc.*, *91*, 95–104.

Hurrell, J., J. Hack, D. Shea, J. Caron, and J. Rosinski (2008), A new sea surface temperature and sea ice boundary dataset for the community atmosphere model, *J. Clim.*, *21*, 5145–5153.
Johnson, S., R. Levine, A. Turner, G. Martin, S. Woolnough, R. Schiemann, and M. Mizielinski (2016), The resolution sensitivity of the South Asian monsoon and Indo-Pacific in a global 0.35 AGCM, *Clim. Dyn.*, *46*, 807–831.
Landu, K., L. Leung, S. Hagos, V. Vinoj, S. Rauscher, T. Ringler, and M. Taylor (2014), The dependence of ITCZ structure on model resolution and dynamical core in aquaplanet simulations, *J. Clim.*, *27*, 2375–2385.
Lenters, J., and K. Cook (1995), Simulation and diagnosis of the regional summertime precipitation climatology of South America, *J. Clim.*, *8*, 2988–3005.
Liu, C., and E. Zipser (2005), Global distribution of convection penetrating the tropical tropopause, *J. Geophys. Res.*, *110*, D23104, doi:10.1029/2005JD006063.
Liu, Y., L. Guo, G. Wu, and Z. Wang (2010), Sensitivity of ITCZ configuration to cumulus convective parameterizations on an aqua planet, *Clim. Dyn.*, *34*, 223–240.
Lucas, C., E. Zipser, and M. LeMone (1994), Vertical velocity in oceanic convection off tropical Australia, *J. Atmos. Sci.*, *51*, 3183–3193.
Marsham, J., N. Dickson, L. Garcia-Carreras, G. Lister, D. Parker, P. Knippertz, and C. Birch (2013), The role of moist convection in the West African monsoon system: Insights from continental-scale convection-permitting simulations, *Geophys. Res. Lett.*, *40*, 1843–1849, doi:10.1002/grl.50347.
Martin, E. R., and C. Thorncroft (2015), Representation of African easterly waves in CMIP5 models, *J. Clim.*, *28*(19), 7702–7715, doi:10.1175/JCLI-D-15-0145.1.
Moebis, B., and B. Stevens (2012), Factors controlling the position of the intertropical convergence zone on an aquaplanet, *J. Adv. Model. Earth Syst.*, *4*, M00A04, doi:10.1029/2012MS000199.
Nordeng, T., (1994), Extended versions of the convection parametrization scheme at ECMWF and their impact upon the mean climate and transient activity of the model in the tropics, *Res. Dept. Tech. Memo. No. 206*, ECMWF, Shinfield Park, Reading, U. K.
Oueslati, B., and G. Bellon (2013), Convective entrainment and large-scale organization of tropical precipitation: Sensitivity of the CNRM-CM5 hierarchy of models, *J. Clim.*, *26*, 2931–2946.
Richter, I., and S. Xie (2008), On the origin of equatorial Atlantic biases in coupled general circulation models, *Clim. Dyn.*, *31*, 587–598.
Rodwell, M. J., and B. J. Hoskins (2001), Subtropical anticyclones and summer monsoons, *J. Clim.*, *14*, 3192–3211.
Roehrig, R., D. Bouniol, and F. Guichard (2013), The present and future of the West African Monsoon: A process-oriented assessment of CMIP5 simulations along the AMMA transect, *J. Clim.*, *26*, 6471–6505.
Schiemann, R., M. Demory, M. Mizielinski, M. Roberts, L. Shaffrey, J. Strachan, and P. Vidale (2013), The sensitivity of the tropical circulation and Maritime Continent precipitation to climate model resolution, *Clim. Dyn.*, *42*, 2455–2468.
Semazzi, F. H. M., and L. Sun (1997), The role of orography in determining the Sahelian climate, *Int. J. Climatol.*, *17*, 581–596.
Siongco, A., C. Hohenegger, and B. Stevens (2015), The Atlantic ITCZ bias in CMIP5 models, *Clim. Dyn.*, *49*, 1169–1180.
Skinner, C. B., and N. S. Diffenbaugh (2013), The contribution of African easterly waves to monsoon precipitation in the CMIP3 ensemble, *J. Geophys. Res. Atmos.*, *118*, 3590–3609, doi:10.1002/jgrd.50363.
Sobel, A., and C. Bretherton (2000), Modeling tropical precipitation in a single column, *J. Clim.*, *13*, 4378–4392.
Song, X., and G. Zhang (2009), Convection parameterization, tropical Pacific double ITCZ, and upper-ocean biases in the NCAR CCSM3. Part I: Climatology and atmospheric feedback, *J. Clim.*, *14*, 4299–4315.
Stein, U., and P. Alpert (1993), Factor separation in numerical simulations, *J. Atmos. Sci.*, *50*, 2107–2115.
Stevens, B., et al. (2013), Atmospheric component of the MPI-M Earth System Model: ECHAM6, *J. Adv. Model. Earth Syst.*, *5*, 146–172, doi:10.1002/jame.20015.
Taylor, C. M., A. Gounou, F. Guichard, P. P. Harris, R. J. Ellis, F. Couvreux, and M. De Kauwe (2011), Frequency of Sahelian storm initiation enhanced over mesoscale soil-moisture patterns, *Nat. Geosci.*, *4*(7), 430–433.
Taylor, K. E., D. Williamson, and F. Zwiers, (2000), The sea surface temperature and sea-ice concentration boundary conditions for AMIP II simulations, PCMDI Rep. 60, Program for Climate Model Diagnosis and Intercomparison, 25 pp., Lawrence Livermore Natl. Lab., Livermore, Calif.
Tian, B., E. Fetzer, B. Kahn, J. Teixeira, E. Manning, and T. Hearty (2013), Evaluating CMIP5 models using AIRS tropospheric air temperature and specific humidity climatology, *J. Geophys. Res. Atmos.*, *118*, 114–134, doi:10.1029/2012JD018607.
Tiedtke, M. (1989), A comprehensive mass flux scheme for cumulus parametrization in large-scale models, *Mon. Weather Rev.*, *117*, 1779–1800.
Turner, J. (1963), The motion of buoyant elements in turbulent surroundings, *J. Fluid Mech.*, *16*, 1–16.
Wernli, H., M. Paulat, M. Hagen, and C. Frei (2008), SAL-A novel quality measure for the verification of quantitative precipitation forecasts, *Mon. Weather Rev.*, *136*, 4470–4487.
Williams, E., and S. Stanfill (2002), The physical origin of the land-ocean contrast in lightning activity, *C.R. Phys.*, *3*, 1227–1292.
Xu, H., Y. Wang, and S. Xie (2004), Effect of the Andes on Eastern Pacific Climate: A regional atmospheric model study, *J. Clim.*, *17*, 589–602.
Xue, Y., et al. (2010), Intercomparison and analyses of the climatology of the West African Monsoon in the West African Monsoon Modeling and Evaluation project (WAMME) first model intercomparison experiment, *Clim. Dyn.*, *35*, 3–28.
Zhao, M., I. M. Held, S.-J. Lin, and G. A. Vecchi (2009), Simulations of global hurricane climatology, interannual variability, and response to global warming using a 50-km resolution gcm, *J. Clim.*, *22*(24), 6653–6678, doi:10.1175/2009JCLI3049.1.
Zipser, E. (2003), Some views on "hot towers" after 50 years of tropical field programs and two years of TRMM data, *Meteorol. Monogr.*, *29*, 49–58.